

LA-UR-14-26735 (Accepted Manuscript)

## Postmidnight depletion of the high-energy tail of the quiet plasmasphere

Sarno-Smith, Lois K  
Liemohn, Michael  
Katus, Roxanne  
Skoug, Ruth M.  
Larsen, Brian Arthur  
Thomsen, Michelle  
Wygant, John  
Moldwin, Mark

Provided by the author(s) and the Los Alamos National Laboratory (2016-02-11).

**To be published in:** JOURNAL OF GEOPHYSICAL RESEARCH-SPACE PHYSICS ; Vol.120, iss.3, p.1646-1660, MAR 2015

**DOI to publisher's version:** 10.1002/2014JA020682

**Permalink to record:** <http://permalink.lanl.gov/object/view?what=info:lanl-repo/lareport/LA-UR-14-26735>

**Disclaimer:**

Approved for public release. Los Alamos National Laboratory, an affirmative action/equal opportunity employer, is operated by the Los Alamos National Security, LLC for the National Nuclear Security Administration of the U.S. Department of Energy under contract DE-AC52-06NA25396. Los Alamos National Laboratory strongly supports academic freedom and a researcher's right to publish; as an institution, however, the Laboratory does not endorse the viewpoint of a publication or guarantee its technical correctness.

# Post-Midnight Depletion of the High Energy Tail of the Quiet Plasmasphere

Lois K. Sarno-Smith<sup>1</sup>, Michael W. Liemohn<sup>1</sup>, Roxanne M. Katus<sup>1</sup>, Ruth M.

Skoug<sup>2</sup>, Brian A. Larsen<sup>2</sup>, Michelle F. Thomsen<sup>3</sup>, John R. Wygant<sup>4</sup>, Mark B.

Moldwin<sup>1</sup>

---

Corresponding author: Lois K. Sarno-Smith, Department of Atmospheric, Oceanic, and Space Sciences, University of Michigan, Ann Arbor, Michigan, USA. (loisks@umich.edu)

<sup>1</sup>Department of Atmospheric, Oceanic,  
and Space Sciences, University of Michigan,  
Ann Arbor, Michigan, USA.

<sup>2</sup>Los Alamos National Laboratory, Los  
Alamos, New Mexico, USA.

<sup>3</sup>Planetary Science Institute, Tucson,  
Arizona, USA.

<sup>4</sup>School of Physics and Astronomy,  
University of Minnesota, Minneapolis,  
Minnesota USA.

This article has been accepted for publication and undergone full peer review but has not been through the copyediting, typesetting, pagination and proofreading process, which may lead to differences between this version and the Version of Record. Please cite this article as doi: 10.1002/2014JA020682

**Abstract.** The Van Allen Probes Helium Oxygen Proton Electron (HOPE)

instrument measures the high energy tail of the thermal plasmasphere allowing study of topside ionosphere and inner magnetosphere coupling. We statistically analyze a 22 month period of HOPE data, looking at quiet times with a Kp index of less than 3. We investigate the high energy range of the plasmasphere, which consists of ions at energies between 1-10 eV and contains approximately 5% of total plasmaspheric density. Both the fluxes and partial plasma densities over this energy range show H<sup>+</sup> is depleted the most in the post-midnight sector (1-4 MLT), followed by O<sup>+</sup> and then He<sup>+</sup>. The relative depletion of each species across the post-midnight sector is not ordered by mass, which reveals ionospheric influence. We compare our results with keV energy electron data from HOPE and the Van Allen Probes Electric Fields and Waves (EFW) instrument spacecraft potential to rule out spacecraft charging. Our conclusion is that the post-midnight ion disappearance is due to diurnal ionospheric temperature variation and charge exchange processes.

## 1. Introduction

The Van Allen Probes mission, launched in August 2012, offers an abundance of unique ion and electron composition measurements of the inner magnetosphere [Lanzerotti, 2013; Mauk *et al.*, 2014]. Recent studies utilizing the Van Allen Probes suite of instruments have augmented our understanding of radiation belt and storm time physics [Reeves *et al.*, 2013; Baker *et al.*, 2013; Usanova *et al.*, 2014]. The Van Allen Probes measurements are also leading to new understanding of the plasmasphere [Goldstein *et al.*, 2014; Li *et al.*, 2013; Jordanova *et al.*, 2014].

The plasmasphere is the dense region of co-rotating plasma near Earth. Some of the first observations of the plasmasphere came from ground-based very low frequency (VLF) measurements looking at sudden changes in whistler wave frequencies [Carpenter *et al.*, 1968; Inan and Bell, 1977; Carpenter *et al.*, 1969]. Recent satellite missions have explored the plasmasphere in much greater detail, including the Imager for Magnetosphere-to-Aurora Global Exploration (IMAGE), Cluster, the Combined Release and Radiation Effects Satellite (CRRES), and the Dynamic Explorer (DE) mission [Burch *et al.*, 2001; Fu *et al.*, 2010; Darrouzet *et al.*, 2009; Carpenter *et al.*, 2000; Horwitz *et al.*, 1990; Chappell *et al.*, 1981].

To motivate the present study of the 1-10 eV ion population of the plasmasphere, we briefly explore other studies examining diurnal temperature and density variation in the plasmasphere and its ionospheric sources. The concentrations of plasmaspheric ions are dependent on energy inputs to the ionosphere, and consequently, ionospheric temperatures. The largest source of sub-auroral ionospheric heating is photoionization.

It has been observed that  $O^+$  and  $H^+$  plasma densities behave similarly to ionospheric electron temperatures on the dayside [*Schunk and Nagy, 1978*].

Plasmaspheric refilling has been extensively studied [*Horwitz, 1987; Carpenter and Lemaire, 1997; Ganguli et al., 2000; Pierrard et al., 2009*]. Transport from the topside ionosphere to the plasmasphere occurs when solar heating of the ionosphere during the day exerts an outward pressure on the topside ionosphere, forcing the ions upward along the flux tubes. Plasma enhancements and depletions with MLT dependence have been modeled in the top-side ionosphere [*Heelis et al., 1982*]. This transport of topside ions applies to all three species, suggesting that the MLT dependence of the  $H^+$ ,  $O^+$ , and  $He^+$  densities might also be seen in the plasmasphere.

The absence of solar heating translates into an absence of pressure on the flux tubes. On the night side, plasmaspheric ions flow downward into the ionosphere, enhancing the nightside NmF2 peak in the ionosphere [*Singh and Singh, 1997; Carpenter and Lemaire, 1997; Pavlov and Pavlova, 2005*]. Collectively, the movement of the high energy ions from the ionosphere to the plasmasphere and then back to the ionosphere on the nightside agrees with temperature measurements of ions and electrons in these regions [*Kotova et al., 2002*].

This diurnal variation is not seen in the thermal core density ( $< 1$  eV) of the plasmasphere. Although many studies and several instruments have explored this region, they have not found a similar result. IMAGE RPI studies looked at fine scale density structures and plasmaspheric electron structures [*Carpenter et al., 2002, 2003; Fu et al., 2010; Denton et al., 2012; Chandler and Chappell, 1986; Ozhogin et al., 2012*], but IMAGE RPI measured total electron number density and was unable to resolve the 1-10

eV energy range to examine density variations. Several physics-based models have also explored plasmaspheric refilling in this region but did not limit their studies to this energy range and did not resolve this diurnal variation [Guiter and Gombosi, 1990; Guiter et al., 1995; Weiss et al., 1997; Liemohn et al., 1997, 1999]. Extensive whistler wave studies have examined electron number densities in the plasmapshe [Carpenter and Anderson, 1992; Park, 1970], but these studies capture, once again, the overall behavior of the plasmasphere instead of our focus on the high energy tail of the plasmasphere. A further discussion of previous measurement techniques of the 1-10 eV plasmasphere population can be found later in the Discussion section.

The Van Allen Probes Mission offers the opportunity to explore the behavior of the high energy (1 - 10 eV) plasmasphere in the  $L < 4$  region at all MLTs to an unprecedented degree. It is critical to study this ion population for understanding magnetosphere-ionosphere coupling and plasmaspheric refilling and for assessing the source, loss, and transport terms between the two regions. The 2-spacecraft Van Allen Probes mission provides an ideal opportunity to study this low energy population of particles, with a short orbital period, a near equatorial orbit, ion composition measurements down to 1 eV, and improved spacecraft potential reduction [Kirby et al., 2014]. In our study, we use the Helium Oxygen Proton Electron (HOPE) instrument on board the Van Allen Probes to explore the quiet time 1-10 eV ion population in the near-Earth plasmasphere and the MLT, L-Shell, and compositional dependencies of this population. We observe a species-dependent loss across all three ion species ( $H^+$ ,  $He^+$ , and  $O^+$ ) in the post-midnight sector near Earth.

## 2. Methodology

This study examines 22 months of quiet time differential number flux measurements from the HOPE instrument on board the Van Allen Probes Mission [Funsten *et al.*, 2013].

HOPE measures  $H^+$ ,  $He^+$ , and  $O^+$  from 1 eV to 50 keV using a time-of-flight mass spectrometer with channel electron multiplier detectors. The 72 HOPE instrument energy channels are logarithmically spaced, with measurements in 5 directions relative to the spin axis and at 16 spin angles. Our study spans from January 2013 to November 2014, which covers a full precession of the Van Allen Probes satellites, and uses gyro and spin averaged data. We used HOPE energies from 1 eV to 10 eV in our study.

To capture the quiet time behavior of the plasmasphere, we included HOPE data collected at times when the Kp Index  $< 3$ . The Kp Index, with a 3 hour cadence, is a mid-latitude index that gives insight into magnetospheric convection and overall geomagnetic activity [Mayaud, 1980; Thomsen, 2004]. Traditionally, a Kp of less than 3 is considered quiet time and corresponds to a Dst greater than -50 nT.

We then binned HOPE fluxes into 0.5 MLT and 0.25 L-Shell bins extending from 1 to 6 L-Shell and 0 to 24 MLT. The L-Shell parameter was calculated using the Olson-Pfizer 77 model [Olson and Pfizer, 1977]. The Van Allen Probes are the first satellite pair to provide high resolution measurements near the equatorial plane with high dwell time inside geosynchronous orbit. Figure 1 shows the number of measurements in each L/MLT bin during the period of this study. We included data from both satellite A and satellite B to maximize coverage. In the post-midnight sector, there are more than 1000 points in each bin, with each point corresponding to an 11 second Van Allen Probe spin measurement. This accumulated to several months of data for each bin. We specifically

show the 2.2 eV energy channel for each species in this figure, but the distributions for the other energy channels between 1-10 eV were similar. The number of measurements for each species corresponds to the number of non-zero measurements; so H<sup>+</sup> measurements from HOPE are the cleanest whereas O<sup>+</sup> has more zero count measurements.

We used the median differential number flux in each L/MLT bin to represent the ions at that location in space. We then calculated approximate plasma densities in each bin using the formula:

$$n_s = \sum_i 4\pi \frac{1}{\sqrt{\frac{2E_i}{m_s}}} F_s(E_i) \Delta E_i \quad (1)$$

where  $F_s(E_i)$  is the median differential number flux (cm<sup>-2</sup> s<sup>-1</sup> sr<sup>-1</sup> keV<sup>-1</sup>),  $E_i$  is the median of each HOPE energy channel,  $\Delta E_i$  represents the range of each energy channel, and  $m_s$  and  $n_s$  are the mass and number density of each species for H<sup>+</sup>, He<sup>+</sup>, and O<sup>+</sup>. The  $i$  in this summation represents the 15 energy channels between 1 eV and 10 eV.

Figure 2 shows the median HOPE flux  $F_s$  for H<sup>+</sup> ions and electrons as a function of energy and MLT for L=2.5 and Kp < 3. This near-Earth location clearly shows the energy spectrum of the plasmasphere at quiet times. A sharp gradient in flux of several orders of magnitude is seen in Figure 2A at approximately 10 eV for most MLTs. This gradient indicates that the plasmasphere is dominated by ions at energies below 10 eV and sets the 10 eV upper boundary for our  $n_s$  density calculations. Integration to higher energies, such as 1 keV, did not change the results except to make the density values slightly higher across all MLT and L-Shells.

It is important to clarify that we are only observing the high energy range of the plasmasphere ion distribution and make no claims on the behavior of the bulk density of the

plasmasphere. Instead, we are looking at the upper 5% (two sigma) of the energy population in the plasmasphere. The expected two sigma energy population of approximately 10-100  $\text{H}^+$  particles  $\text{cm}^{-3}$  for the plasmaspheric high energy tail is consistent with the total plasmaspheric densities given by CRRES data-based models at  $L=2$  [Sheeley *et al.*, 2001]. A further discussion of this can be found in Appendix A. A discussion of spacecraft charging effects on our measurements can be found in section 4.2.

### 3. Results

When we examine partial plasma densities across all MLTs and L-Shells, we find a significant density depletion across the post-midnight sector. Figure 3 shows the median plasma density of quiet time 1-10 eV ions measured by HOPE over a 22 month period. Figure 3A shows the  $\text{H}^+$  density across all MLTs and L-Shells, Figure 3B gives the  $\text{He}^+$  density, and Figure 3C shows the  $\text{O}^+$  plasma density. The density maps on the right are on a logarithmic scale, while the maps on the left are on a relative linear scale for each species to highlight changes. We see in Figure 3B that  $\text{He}^+$  behaves differently than  $\text{O}^+$  and  $\text{H}^+$ , with a gradual decline and ascent in density over the post-midnight sector. In  $\text{He}^+$  density, a local minimum is seen at  $\text{MLT}=14$  and is suggested to be from a saturation feedback mechanism [Galvan *et al.*, 2008].

Although the  $\text{He}^+$  density decreases post-midnight, it does not drop to the same degree as  $\text{O}^+$  and  $\text{H}^+$ , as evidenced by the percentage each ion species contributes to the total partial plasma density. Figure 4 shows the relative contribution of each species to the total ion density in the 1-10 eV energy range.  $\text{H}^+$  dominates everywhere (upwards of 60%) except in two regions. One is the post-midnight depletion zone, where  $\text{He}^+$  has a strong presence and makes up more than 50% of the total plasma density.

We can see in the ion composition percentages that  $\text{He}^+$  dominates the 1-10 eV plasma density at  $\text{MLT}=0-5$  and  $L < 2.5$ . This result is counterintuitive because  $\text{He}^+$  is heavier than  $\text{H}^+$  and lighter than  $\text{O}^+$ , so the effect is not organized by mass in this energy range.

To emphasize this result, we examine the partial plasma density gradient across all MLTs at  $L=2.0$ . Figure 5 shows a line plot of partial densities at  $L=2.0$ . Specifically, we calculated the average density values for each species from 2-4 MLT and 14-16 MLT. We found that the  $\text{H}^+$  density was  $55.8 \text{ cm}^{-3}$  at  $\text{MLT}=18$  and  $0.37 \text{ cm}^{-3}$  at  $\text{MLT}=3$  (a factor of 150). The  $\text{He}^+$  density was  $7.18 \text{ cm}^{-3}$  at  $\text{MLT}=18$  and  $0.26 \text{ cm}^{-3}$  at  $\text{MLT}=3$  (a factor of 28). The  $\text{O}^+$  density was  $7.74 \text{ cm}^{-3}$  at  $\text{MLT}=18$  and  $0.06 \text{ cm}^{-3}$  at  $\text{MLT}=3$  (a factor of 122). In  $\text{He}^+$ , the drop is still distinct, but it is not nearly as great as  $\text{O}^+$  or  $\text{H}^+$  across the same MLTs. These results demonstrate that there is a depletion in all species, but the effect is most pronounced in  $\text{H}^+$  and  $\text{O}^+$ .

To better understand the variation in the data set, we explore the 33rd and 66th percentile of each flux bin in Figure 6 and the relative standard deviation and spread of the data in Figure 7. By examining the 33rd and 66th percentile of the 2.2 eV differential number flux, we can see that the post-midnight feature is consistent throughout the data set and the median of the each of the flux bins is reflecting the general behavior of the dataset well.

The left column of Figure 7 shows the relative standard deviation. Although the relative standard deviation of the post-midnight sector is high compared to other regions, the right column clarifies the spread in the data. The scatter plots in the right column show the differential number fluxes for both satellites for energy channel 2.2 eV of the  $L = 2.0$  bin for  $\text{MLT}=3, 9, 15$ , and 21. The dayside and pre-midnight MLTs have considerably less

variation than MLT=3, but these MLT values also have consistently higher flux values than the MLT=3 measurements. The geometric factor for HOPE is  $10^{-3} \text{ cm}^2 \text{ sr}$  at 1 eV [Funsten *et al.*, 2013] so the  $10^5$  flux measurements for HOPE are close to the 1 count level. From Figure 7 we can conclude that there is more variation in the post-midnight sector, but the measured fluxes themselves fall within a certain range which is consistently below the dayside and pre-midnight MLTs.

To confirm the statistical results shown in Figures 3 - 7, we also looked at case studies of individual events. Figure 8 shows the HOPE fluxes from 1-7000 eV for a 6 hour period on April 30, 2013. HOPE passes through the post-midnight sector at low L-Shell and sees a drop in flux values for  $\text{H}^+$ . A dip in flux is seen at all energies up to 10 keV, and the lowered flux measurements are consistent across the satellite transitioning from the inbound to outbound path. The bottom panel of Figure 8 shows the spacecraft potential from EFW ranged from 0 V to 0.75 V in the post-midnight,  $L < 3$  sector. There is clear sensitivity to spacecraft potential fluctuations in the lower energy channels, but the flux dip in the post-midnight, low L-Shell region is seen at energies above sensitivity to spacecraft charging (e.g., 1 keV). The behavior of the ions shown in the case study suggests that the density drop is indicative of a dramatic plasma temperature change. This behavior correlates well with ionospheric electron and ion temperatures across the nightside [Pavlov and Pavlova, 2005].

To determine whether the post-midnight depletion in the 1-10 eV energy range is a density loss or a cooling effect, we compared the median flux measurements as a function of energy at  $L=2.0$  at MLT=3,9,15, and 21. Figure 9 shows these results, where the energy values have been shifted by 0.75 eV to account for the average impact of positive

spacecraft charging (0.75 eV) on HOPE measurements. The slopes of the lines in Figure 9 indicate the change in the distribution with energy and follow an approximately Maxwellian distribution. We find that the distributions from all MLTs have about the same slope, but the MLT=3 median measurements show lower flux. However, based on this limited range (1-10 eV) of the distribution, we are unable to definitely state whether this is purely a temperature change or a density loss.

#### 4. Discussion

Through statistical analysis and a case study example, we have demonstrated that there is a depletion across  $H^+$ ,  $He^+$ , and  $O^+$  in the post-midnight sector as seen by the HOPE instrument in the upper end of the thermal distribution of the plasmasphere. Further, the compositional dependence of the nightside loss is that  $H^+$  is depleted the most, followed by  $O^+$ , and then  $He^+$ ; thus the depletion is not ordered by particle mass. A physical explanation of this unusual result is given below, along with an analysis of spacecraft charging, which is an issue of critical importance to the veracity of the findings for the quiet time 1-10 eV population.

##### 4.1. Diurnal Variation Analysis

This variation with species can be explained by observing that plasmaspheric ions at these energies come from the dayside ionosphere [Chappell *et al.*, 1987]. The  $He^+$  density profile is similar to the ion temperature profile of the ionosphere [Roble, 1975]. The double peak feature of  $He^+$  at pre-noon and dusk is similarly seen in the work of Galvan *et al.* [2008]. They concluded this feature is due to a local minimum in the topside ionospheric

ion density at noon, and thus, with an ionospheric source for 1-10 eV plasma, then the density decrease in plasmaspheric  $\text{He}^+$  is consistent.

The MLT dependent behavior of the high energy plasmasphere tail comes from the production of  $\text{H}^+$ ,  $\text{O}^+$ , and  $\text{He}^+$  in the top side ionosphere.  $\text{H}^+$  and  $\text{O}^+$  have accidental charge resonance,



This linked reaction is responsible for the tandem behavior of  $\text{H}^+$  and  $\text{O}^+$  in the high energy portion of the plasmasphere. In particular,  $S_{\text{H}^+}$ , the source of  $\text{H}^+$ , is given by,

$$S_{\text{H}^+} = m_{\text{H}} \sigma_e \sqrt{\frac{8kT_n}{\pi m_{\text{H}}}} n(\text{O}^+) n(\text{H}) \quad (3)$$

where  $\sigma_e$ , the electron collisional cross section, is approximately  $2 \times 10^{-15} \text{ cm}^2$ . So as the neutral temperature,  $T_n$ , increases due to heating from photoionization when in the post dawn sector, the  $\text{H}^+$  population grows.  $\text{He}^+$  is also produced in the ionosphere from solar radiation with  $\lambda < 50.4 \text{ nm}$ . The dominant loss mechanism for  $\text{He}^+$  is charge transfer with the neutrals  $\text{O}_2$  and  $\text{N}_2$ , which are extremely rarefied in the topside ionosphere.

Since the source of  $\text{H}^+$  is sensitive to thermospheric temperature, which is demonstrated in (3), and since  $\text{O}^+$  is tied to  $\text{H}^+$  via (4), these populations will naturally decline after the terminator due to the cooling of the atmosphere.  $\text{He}^+$  production is sensitive to solar exposure but has a longer loss/gain timescale than that of  $\text{O}^+$  and  $\text{H}^+$  and consequently shows a less dramatic density depletion.

The diurnal variation of  $H^+$  is seen in the topside ionosphere from previous studies [*Ho et al.*, 1971; *Richards et al.*, 1985]. The topside ionosphere temperature minimum occurs between 0-4 local time and peaks in the afternoon. This variation supports our claim that near-Earth 1-10 eV plasmasphere ions exhibit similar behavior to topside ionosphere ions.

## 4.2. Spacecraft Charging

Surface spacecraft charging in a lower density and higher energy plasma affects measurements by shifting the energy distribution function of a plasma by the potential energy,  $e\phi$ . So, if HOPE makes a measurement at 2 eV, but there is 1.5 V of spacecraft charging, then these measured 2 eV ions would actually have been 0.5 eV ions (2 eV - 1.5 eV) because they are accelerated toward the negatively charged satellite. Likewise, if there is a positive potential, the ion population observed by HOPE would appear to be lower energy than the actual distribution [*Garrett*, 1981].

The post-midnight sector is notorious for spacecraft charging effects, particularly for satellites in geosynchronous orbit. *Mizera and Boyd* [1982] explore this topic from an engineering perspective, using the USAF P78-2 satellite to calibrate spacecraft charging based on materials used, Kp, and MLT as a function of percentage of satellite affected. They found that at geosynchronous orbit, spacecraft charging, particularly in the post-midnight sector, is high during times of high and low Kp. For within geosynchronous orbit, a small percentage of the total time (< 3%), there is spacecraft charging in the post-midnight sector; however, an equivalent amount of charging is seen post dawn, in which our results are unaffected.

To calibrate how much spacecraft charging occurs in the post-midnight sector relative to other MLTs and determine if our results might be biased by spacecraft charging, we

used the Van Allen Probes Electric and Magnetic Field Instrument Suite and Integrated Science (EMFISIS) instrument [Kletzing *et al.*, 2014], and the Electric Fields and Waves (EFW) instrument [Wygant *et al.*, 2014]. Using EFW spacecraft potential for the entirety of the Van Allen Probes Mission (November 2012 to April 2014), we binned spacecraft potential by 0.25 L-Shell and 0.5 MLT and then took the median of each bin, which is shown in Figure 10. We did not sort spacecraft potential by Kp index because very few storms occurred in this time period.

In Figure 10A, we can see that the spacecraft potential is less positive in Earth's shadow (e.g., at L=2, the median potential is 0.65 V at 18 MLT, but only 0.15 V at 0 MLT). The lower potential indicates that ions near midnight are decelerated by a smaller amount as they approach the detector. Our statistical study of spacecraft potential shows little difference in spacecraft potential between the post-midnight sector and the dusk sector, yet we see a dramatic difference in the partial plasma density maps of Figure 3.

We supplement Figure 10A with a variation analysis shown in B. The relative standard deviation is the standard deviation of spacecraft potential measurements within a bin divided by the mean spacecraft potential of that bin. The relative standard deviation is approximately constant across low L-Shell MLTs, but at high L-Shells ( $> 3$ ), there is more variation in the post-midnight sector. This is expected because of the eastward gradient curvature drift of high-energy electrons, which would increase spacecraft charging. However, this effect does not penetrate to lower L-Shells because the electrons drift eastward before they can reach that close to Earth, especially for the  $Kp < 3$  quiet time data selection filter applied for this study.

Furthermore, Figure 11 directly compares the median spacecraft potentials at MLT=3 and MLT=18 with the median densities at these same local times. From  $L=1.75$  to  $L=2.5$ , the spacecraft potentials in these two regions are nearly identical, while the densities differ by an order of magnitude with a density of  $10\text{ cm}^{-3}$  at MLT=18 and  $1\text{ cm}^{-3}$  at MLT=3. Beyond  $L=2.5$ , the spacecraft potentials at the two local times diverge with a higher potential observed at MLT=18. However, the density at MLT=3 remains lower than the density at MLT=18 out to at least  $L=4$ . This figure directly shows that the ion loss in the post-midnight sector is not related to higher spacecraft potentials in this region.

We also examine the HOPE electron measurements at  $L=2$ , shown in Figure 2B, for any observable difference in the post-midnight sector compared to other MLTs. We do see a slight increase in median electron flux measurements in the post-midnight sector; however, there is also a comparable sized electron flux augmentation at 15:00 MLT, ruling out this electron intensity increase as responsible for the ion depletion. Also, the HOPE low-energy electron densities are highest at post-dawn, supporting our interpretation that electrons, produced from photoionization in the ionosphere and then scattered at high altitudes on these field lines, mirror and deposit their energy and warm the plasmasphere.

Due to the maximum frequency on EMFISIS of 400 kHz, the EMFISIS electron number density measurements saturate at  $L < 3$ , making it impossible to distinguish differences between MLT electron number densities at low L-Shells. This prevents us from determining if the electron number densities also exhibit a similar drop as the ion plasma densities across the post-midnight sector using Van Allen Probes data.

### 4.3. Why This Depletion Has Not Been Previously Observed

In examining the 1-10 eV population in Van Allen Probes data, we questioned why this effect was not observed by previous missions. The uniqueness of the Van Allen Probes mission allowed for clear observation of this post-midnight density loss. In the following section we specifically address why this loss was not observed in other missions and a brief description of those missions.

IMAGE EUV visualized the plasmasphere by counting solar EUV photons resonantly scattered with  $\text{He}^+$  [Sandel *et al.*, 2000, 2001], producing vivid pictures of the plasmasphere and highlighting the plasmaspheric plume [Spasojević *et al.*, 2004]. These results are somewhat limited, as IMAGE EUV gives an integrated total density over a line of sight and utilizes an inversion procedure to provide local density values [Gurgiolo *et al.*, 2005]. The IMAGE radio plasma imager (RPI) allowed for electron density measurements along plasmaspheric field lines and distributions from the polar cap ionosphere [Reinisch *et al.*, 2000, 2001]. However, IMAGE EUV only measured total  $\text{He}^+$  densities, which overshadows the plasma loss in the 1-10 eV range.

The Cluster mission offered the advantage of a polar orbit that ultimately transformed into an equatorial orbit [Escoubet *et al.*, 1999, 2013] and the Cluster Ion Spectroscopy (CIS) instrument that measured composition [Reme *et al.*, 2001]. However, the Cluster CIS-CODIF measured  $> 40$  eV ions, which is above our study's energy range. Also, the Cluster perigee is at approximately  $L=4$ , and our study focuses on the region between  $L=2$  and  $L=3$ . The Waves of High frequency and Sounder for Probing of Electron density by Relaxation (WHISPER) experiment on board Cluster provided electron density

measurements and total plasma density measurements within  $0.2\text{--}80\text{ cm}^{-3}$  [Décréau *et al.*, 1997], which is useful for understanding plasma distribution outside of an L-Shell of 4.

The Combined Release and Radiation Effects Satellite (CRRES) also provided ample information about the behavior of the plasmasphere. From upper hybrid resonance frequency measurements, CRRES captured the behavior of plasmaspheric electron density exceptionally well, documenting the plasmasphere trough with precision [Sheeley *et al.*, 2001; Moldwin *et al.*, 2002]. The mission goals of CRRES were to better understand the radiation environment near Earth and perform several chemical release experiments; however, this satellite was not able to measure low energy plasma due to instrumentation difficulties [Johnson and Kierein, 1992] and CRRES did not directly measure ion composition.

The Retarding Ion Mass Spectrometer (RIMS) onboard Dynamics Explorer 1 (DE-1) [Chappell *et al.*, 1981] measured ion composition from 0-50 eV for  $\text{H}^+$ ,  $\text{He}^+$ , and  $\text{O}^+$ . With a polar orbit and an apogee at 4 Earth radii, DE-1 provided a wealth of information of near Earth plasma, low energy ion composition, such as the presence of the warm plasma cloak [Chappell *et al.*, 2008] and provided the basis for initial plasmasphere models [Gallagher *et al.*, 1988]. This effect was not reported in results of the RIMS data set, but RIMS data could be used to confirm the results seen here. The High Altitude Plasma Instrument (HAPI) onboard DE-1 provided measurements on the velocity space distribution of ion and electrons from 5 eV to 32 keV near Earth [Burch *et al.*, 1981; Winningham *et al.*, 1981].

However, HAPI did not distinguish composition and focused on plasma injections into the polar region [Burch *et al.*, 1982; Newell *et al.*, 1991]. DE-2 observations built on our

understanding of topside ionospheric electron temperatures [Kozyra *et al.*, 1986]. However, the DE-2 satellite was an ionospheric polar orbiter and did not fly at high enough altitudes to see the low energy ion population at  $L > 2$ .

A combination unique to all of these missions, Van Allen Probes offers high dwell time in the inner magnetosphere, a near equatorial orbit, and the ability to distinguish the 1-10 eV ion population cleanly.

## 5. Conclusions

Using the HOPE instrument data to look at plasma density for  $H^+$ ,  $He^+$ , and  $O^+$  from 1 - 10 eV during quiet time periods, we see strong MLT dependence in the high energy tail of the plasmasphere. Our study has two main findings: there is diurnal variation across all three ion species in the 1-10 eV range and there is a compositional difference in the amount of loss observed across the post-midnight sector.

We observed that  $H^+$ ,  $He^+$ , and  $O^+$  decrease rapidly, similar to ionospheric temperatures across the nightside. We propose that all three species experience rapid density gains at the dawn terminator because the dayside plasmasphere heats quickly from the magnetic mirroring and energy loss of electrons scattered from photoionization from neutrals. This thermalization of the plasmasphere energizes the ions over the course of a couple of hours, which is what we observe across the dawn terminator in Figure 3.

We see that  $He^+$  loss is the smallest, as supported by Figure 5.  $H^+$  and  $O^+$  densities follow each other closely because of the charge resonance that exists between these two species. So when  $H^+$  is lost faster than  $He^+$  and  $O^+$  because of its low mass, the net effect is a rapid combined loss of  $H^+$  and  $O^+$  because of their tandem behavior. The enhanced high energy densities from photoionization in these ions remains throughout the day, and

then declines slowly after the dusk terminator. The populations almost vanish in the post-midnight sector, with density values dropping a factor of 28 to 150 (Figure 5).

$\text{He}^+$  in the high energy plasmasphere tail exhibits different MLT dependence than  $\text{H}^+$  and  $\text{O}^+$ . The source of ionospheric  $\text{He}^+$  is photoionization, which peaks in the morning sector and then again at dusk. The increase of dayside  $\text{He}^+$  is thought to be from the day-side warm ionosphere exerting a pressure on  $\text{He}^+$  ions, pushing them into plasmaspheric flux tubes. The decline in  $\text{He}^+$  on the nightside, particularly in the post-midnight sector, is still significant at a factor of 28 but is not as sharp as  $\text{H}^+$  and  $\text{O}^+$ .  $\text{He}^+$ , although lighter than  $\text{O}^+$ , has a slower loss rate because of the  $\text{O}^+$  charge resonance with  $\text{H}^+$ .

This study shows the MLT dependence of high energy plasmasphere ions seen in the HOPE instrument on the Van Allen Probes during quiet time intervals. Unanswered questions on the ions in this regime still remain, such as what causes the local minimum of  $\text{He}^+$  in the ionosphere and in the high energy ion tail of the plasmasphere. Also, we have not investigated how periods of high convection or how binning by other indices, such as Dst, may shed additional light on physics behind the 1-10 eV partial plasma density depletion in the post-midnight sector.

## **Appendix A: Comparison of HOPE Data to Modeled Plasmasphere Data**

Since most plasmasphere particles have low energy ( $< 1$  eV) and the HOPE solid angle has viewing gaps, the HOPE energy range covers only a fraction of the total plasmaspheric distribution. To place the HOPE measurements in the context of previous observations, we wish to confirm that the 1-10 eV quiet time HOPE partial densities are consistent with the total plasma density measured by previous missions by calculating what fraction of the total plasma density distribution the HOPE energy range expects to measure. To do

this, we assume that the energy distribution of the plasmasphere can be represented as a Maxwellian,

$$F_m = n_0 \left( \frac{m_s}{kT} \right)^{3/2} 4\pi e^{-E_n/kT} \frac{1}{\sqrt{2m_s E_n}} \frac{2E_n}{m_s} \quad (\text{A1})$$

where  $F_m$  is the differential number flux,  $m$  is the mass of the ion species,  $k$  is Boltzmann's constant,  $n_0$  is the total number density,  $T$  is the plasma temperature, and  $E_n$  is the plasma energy. We find the partial density of this energy range by integrating over the Maxwell-Boltzmann distribution of ion energies from 1-10 eV,

$$n = \int F_m dE_n \quad (\text{A2})$$

For simplicity, we perform this calculation at  $L=2$ , where the total plasmaspheric  $H^+$  density is approximately  $1800 \text{ cm}^{-3}$  [Chappell, 1972; Gallagher et al., 1988]. Also in (A1),  $T$  is the median temperature of the plasmasphere taken from Comfort et al. [1985]. In Figure A1, we show the differential number flux for different plasmaspheric temperatures [Comfort et al., 1985]. The high energy tail of the plasmasphere is the area under the curve past the dotted black line, comprising approximately 5% of the total density. Our integrating variable,  $E_n$ , is the bounding energies of the fraction of the Maxwellian that we want to calculate the density,  $n$ , in this case 1 - 10 eV. To confirm this  $n_0$  value we also checked the empirical relationship for electron number densities given in Carpenter and Anderson [1992] based on L-Shell value and then using Gallagher et al. [2000] to estimate  $H^+$  density as most of the plasmasphere mass at  $L=2$ . The value given through this method for  $n_e$  at  $L=2$  was  $1866 \text{ cm}^{-3}$ , which will be approximately equal to  $n_{H^+}$ .

**Acknowledgments.** The authors would like to thank Roger Varney, Daniel Welling, Shaosui Xu, Rick Chappell, and Raluca Ilie for their insights and contributions to this work. The Michigan co-authors would like to thank the University of Michigan Rackham Graduate school, NASA, and the NSF for sponsoring this work under grants NWX11AO60G, NWX144AC02G, and AGS-1102863. Work at Los Alamos National Laboratory was performed under the auspices of the U.S. Department of Energy, with support from the NASA Van Allen Probes mission. Data used to generate figures for this project came from the Van Allen Probes data center at [http://www.rbsp-ect.lanl.gov/data\\_pub/](http://www.rbsp-ect.lanl.gov/data_pub/) and the Kyoto World Data Center for geomagnetism at <http://wdc.kugi.kyoto-u.ac.jp/>, with the exception of the spacecraft potential which was provided by Dr. John Wygant upon request. The authors would also like to thank Dennis Gallagher and K.J. Genestreti for insights and contributions in reviewing this paper.

## References

- Baker, D., S. Kanekal, V. Hoxie, M. Henderson, X. Li, H. E. Spence, S. Elkington, R. Friedel, J. Goldstein, M. Hudson, et al. (2013), A long-lived relativistic electron storage ring embedded in Earth's outer Van Allen belt, *Science*, *340*(6129), 186–190.
- Burch, J., J. Winningham, V. Blevins, N. Eaker, W. Gibson, and R. Hoffman (1981), High-altitude plasma instrument for Dynamics Explorer-A, *Space Science Instrumentation*, *5*, 455–463.
- Burch, J., P. Reiff, R. Heelis, J. Winningham, W. Hanson, C. Gurgiolo, J. Menietti, R. Hoffman, and J. Barfield (1982), Plasma injection and transport in the mid-altitude polar cusp, *Geophysical Research Letters*, *9*(9), 921–924.

Burch, J., S. Mende, D. Mitchell, T. Moore, C. Pollock, B. Reinisch, B. Sandel, S. Fuselier, D. Gallagher, J. Green, et al. (2001), Views of Earth's Magnetosphere with the IMAGE Satellite, *Science*, 291(5504), 619–624.

Carpenter, D., and R. Anderson (1992), An ISEE/Whistler model of equatorial electron density in the magnetosphere, *Journal of Geophysical Research: Space Physics (1978–2012)*, 97(A2), 1097–1108.

Carpenter, D., F. Walter, R. Barrington, and D. McEwen (1968), Alouette 1 and 2 Observations of abrupt changes in Whistler rate and of VLF noise variations at the plasma-pause - A satellite-ground study, *Journal of Geophysical Research*, 73(9), 2929–2940.

Carpenter, D., C. Park, H. Taylor, and H. Brinton (1969), Multi-experiment detection of the plasmopause from EOGO satellites and antarctic ground stations, *Journal of Geophysical Research*, 74(7), 1837–1847.

Carpenter, D., T. Bell, U. Inan, R. Benson, V. Sonwalkar, B. Reinisch, and D. Gallagher (2003), Z-mode sounding within propagation cavities and other inner magnetospheric regions by the RPI instrument on the IMAGE satellite, *Journal of Geophysical Research: Space Physics (1978–2012)*, 108(A12).

Carpenter, D. L., and J. Lemaire (1997), Erosion and recovery of the plasmasphere in the plasmopause region, *Space Science Reviews*, 80(1-2), 153–179.

Carpenter, D. L., R. Anderson, W. Calvert, and M. Moldwin (2000), CRRES observations of density cavities inside the plasmasphere, *Journal of Geophysical Research: Space Physics (1978–2012)*, 105(A10), 23,323–23,338.

Carpenter, D. L., M. Spasojević, T. F. Bell, U. S. Inan, B. W. Reinisch, I. Galkin, R. F. Benson, J. Green, S. F. Fung, and S. Boardsen (2002), Small-scale field-aligned plasma-

spheric density structures inferred from the Radio Plasma Imager on IMAGE, *Journal of Geophysical Research: Space Physics* (1978–2012), 107(A9), SMP–22.

Chandler, M., and C. Chappell (1986), Observations of the flow of  $H^+$  and  $He^+$  along magnetic field lines in the plasmasphere, *Journal of Geophysical Research: Space Physics* (1978–2012), 91(A8), 8847–8860.

Chappell, C. (1972), Recent satellite measurements of the morphology and dynamics of the plasmasphere, *Reviews of Geophysics*, 10(4), 951–979.

Chappell, C., S. Fields, C. Baugher, J. Hoffman, W. Hanson, W. Wright, H. Hammack, G. Carignan, and A. Nagy (1981), The Retarding Ion Mass Spectrometer on Dynamics Explorer-A, *Space Science Instrumentation*, 1.

Chappell, C., T. Moore, and J. Waite (1987), The ionosphere as a fully adequate source of plasma for the Earth's magnetosphere, *Journal of Geophysical Research: Space Physics* (1978–2012), 92(A6), 5896–5910.

Chappell, C., M. Huddleston, T. Moore, B. Giles, and D. Delcourt (2008), Observations of the warm plasma cloak and an explanation of its formation in the magnetosphere, *Journal of Geophysical Research: Space Physics* (1978–2012), 113(A9).

Comfort, R. H., J. H. Waite, and C. R. Chappell (1985), Thermal ion temperatures from the Retarding Ion Mass Spectrometer on DE-1, *Journal of Geophysical Research: Space Physics*, 90(A4), 3475–3486, doi:10.1029/JA090iA04p03475.

Darrouzet, F., D. L. Gallagher, N. André, D. L. Carpenter, I. Dandouras, P. M. Décréau, J. De Keyser, R. E. Denton, J. C. Foster, J. Goldstein, et al. (2009), Plasmaspheric density structures and dynamics: Properties observed by the Cluster and IMAGE missions, in *The Earth's Plasmasphere*, pp. 55–106, Springer.

Décréau, P., P. Ferreau, V. Krannosels' kikh, M. Lévêque, P. Martin, O. Randriamboarison, F. Sené, J. Trotignon, P. Canu, and P. Mögensen (1997), WHISPER, a resonance sounder and wave analyser: Performances and perspectives for the Cluster mission, *Space Science Reviews*, 79(1-2), 157–193.

Denton, R., Y. Wang, P. Webb, P. Tengdin, J. Goldstein, J. Redfern, and B. Reinisch (2012), Magnetospheric electron density long-term (> 1 day) refilling rates inferred from passive radio emissions measured by IMAGE RPI during geomagnetically quiet times, *Journal of Geophysical Research: Space Physics* (1978–2012), 117(A3).

Escoubet, C., M. Fehringer, and M. Goldstein (1999), Introduction the Cluster mission, in *Annales Geophysicae*, vol. 19, pp. 1197–1200, Copernicus GmbH.

Escoubet, C., M. Taylor, A. Masson, H. Laakso, J. Volpp, M. Hapgood, and M. Goldstein (2013), Dynamical processes in space: Cluster results, in *Annales Geophysicae*, vol. 31, pp. 1045–1059.

Fu, H., J. Tu, J. Cao, P. Song, B. Reinisch, D. Gallagher, and B. Yang (2010), IMAGE and DMSP observations of a density trough inside the plasmasphere, *Journal of Geophysical Research: Space Physics* (1978–2012), 115(A7).

Funsten, H., R. Skoug, A. Guthrie, E. MacDonald, J. Baldonado, R. Harper, K. Henderson, K. Kihara, J. Lake, B. Larsen, A. Puckett, V. Vigil, R. Friedel, M. Henderson, J. Niehof, G. Reeves, M. Thomsen, J. Hanley, D. George, J.-M. Jahn, S. Cortinas, A. De Los Santos, G. Dunn, E. Edlund, M. Ferris, M. Freeman, M. Maple, C. Nunez, T. Taylor, W. Toczynski, C. Urdiales, H. Spence, J. Cravens, L. Suther, and J. Chen (2013), Helium, Oxygen, Proton, and Electron (HOPE) mass spectrometer for the Radiation Belt Storm Probes mission, *Space Science Reviews*, 179(1-4), 423–484, doi:

10.1007/s11214-013-9968-7.

Gallagher, D., P. Craven, and R. Comfort (1988), An empirical model of the Earth's plasmasphere, *Advances in Space Research*, 8(8), 15–24.

Gallagher, D. L., P. D. Craven, and R. H. Comfort (2000), Global core plasma model, *Journal of Geophysical Research: Space Physics (1978–2012)*, 105(A8), 18,819–18,833.

Galvan, D. A., M. B. Moldwin, and B. R. Sandel (2008), Diurnal variation in plasmaspheric  $\text{He}^+$  inferred from extreme ultraviolet images, *Journal of Geophysical Research: Space Physics (1978–2012)*, 113(A9).

Ganguli, G., Reynolds, M. A., Liemohn, M. W. (2000), The plasmasphere and advances in plasma spheric research , *Journal of Atmospheric and Solar-Terrestrial Physics*, 62(17), 1647–1657.

Garrett, H. B. (1981), The charging of spacecraft surfaces, *Reviews of Geophysics*, 19(4), 577–616.

Garrett, H. B. (1981), The charging of spacecraft surfaces, *Reviews of Geophysics*, 19(4), 577–616.

Goldstein, J., M. Spasojević, P. Reiff, B. Sandel, W. Forrester, D. Gallagher, and B. Reinisch (2003), Identifying the plasmopause in IMAGE EUV data using IMAGE RPI in situ steep density gradients, *Journal of Geophysical Research: Space Physics (1978–2012)*, 108(A4).

Goldstein, J., S. De Pascuale, C. Kletzing, W. Kurth, K. J. Genestreti, R. M. Skoug, B. A. Larsen, L. M. Kistler, C. Mouikis, and H. Spence (2014), Simulation of Van Allen Probes Plasmopause Encounters, *Journal of Geophysical Research: Space Physics (2014)*.

Guiter, S., and T. Gombosi (1990), The role of high-speed plasma flows in plasmaspheric refilling, *Journal of Geophysical Research: Space Physics* (1978–2012), *95*(A7), 10,427–10,440.

Guiter, S., T. I. Gombosi, and C. Rasmussen (1995), Two-stream modeling of plasmaspheric refilling, *Journal of Geophysical Research: Space Physics* (1978–2012), *100*(A6), 9519–9526.

Gurgiolo, C., B. Sandel, J. Perez, D. Mitchell, C. Pollock, and B. Larsen (2005), Overlap of the plasmasphere and ring current: Relation to subauroral ionospheric heating, *Journal of Geophysical Research: Space Physics* (1978–2012), *110*(A12).

Heelis, RA, Jo K Lowell, and Ro W. Spiro (1982), A model of the high-latitude ionospheric convection pattern , *Journal of Geophysical Research: Space Physics* (1978–2012), *87*(A8).

Ho, MC and DR Moorcroft (1971), Hydrogen density and proton flux in the topside ionosphere over Arecibo, Puerto Rico, from incoherent scatter observations, *Planetary and Space Science*, *19*(11), 1441-1455.

Horwitz, J. (1987), Core Plasma in the Magnetosphere , *Reviews of Geophysics* (1978–2012), *25*(A2), 579–587.

Horwitz, J., R. Comfort, and C. Chappell (1990), A statistical characterization of plasmasphere density structure and boundary locations, *Journal of Geophysical Research: Space Physics* (1978–2012), *95*(A6), 7937–7947.

Inan, U. S., and T. F. Bell (1977), The plasmopause as a VLF wave guide, *Journal of Geophysical Research*, *82*(19), 2819–2827.

- Johnson, M., and J. Kierein (1992), Combined Release and Radiation Effects Satellite (CRRES): Spacecraft and mission, *Journal of Spacecraft and Rockets*, *29*(4), 556–563.
- Jordanova, V., Y. Yu, J. Niehof, R. Skoug, G. Reeves, C. Kletzing, J. Fennell, and H. Spence (2014), Simulations of inner magnetosphere dynamics with an expanded RAM-SCB model and comparisons with Van Allen Probes observations, *Geophysical Research Letters*, *41*(8), 2687–2694.
- Kirby, K., D. Artis, S. Bushman, M. Butler, R. Conde, S. Cooper, K. Fretz, C. Herrmann, A. Hill, J. Kelley, et al. (2014), Radiation Belt Storm Probes Observatory and Environments, in *The Van Allen Probes Mission*, pp. 59–125, Springer.
- Kletzing, C., W. Kurth, M. Acuna, R. MacDowall, R. Torbert, T. Averkamp, D. Bodet, S. Bounds, M. Chutter, J. Connerney, et al. (2014), The Electric and Magnetic Field Instrument Suite and Integrated Science (EMFISIS) on RBSP, in *The Van Allen Probes Mission*, pp. 127–181, Springer.
- Kotova, G., V. Bezrukikh, M. Verigin, and L. Lezhen (2002), Temperature and density variations in the dusk and dawn plasmasphere as observed by Interball Tail in 1999–2000, *Advances in Space Research*, *30*(7), 1831–1834.
- Kozyra, J., L. Brace, T. Cravens, and A. Nagy (1986), A statistical study of the subauroral electron temperature enhancement using Dynamics Explorer 2 langmuir probe observations, *Journal of Geophysical Research: Space Physics (1978–2012)*, *91*(A10), 11,270–11,280.
- Lanzerotti, L. J. (2013), Van Allen Probes mission, *Space Weather*, *11*(4), 133–133, doi: 10.1002/swe.20037.

- Lawrence, D., M. Thomsen, J. Borovsky, and D. McComas (1999), Measurements of early and late time plasmasphere refilling as observed from geosynchronous orbit, *Journal of Geophysical Research: Space Physics* (1978–2012), 104(A7), 14,691–14,704.
- Li, W., R. Thorne, J. Bortnik, G. Reeves, C. Kletzing, W. Kurth, G. Hospodarsky, H. E. Spence, J. Blake, J. Fennell, et al. (2013), An unusual enhancement of low-frequency plasmaspheric hiss in the outer plasmasphere associated with substorm-injected electrons, *Geophysical Research Letters*, 40(15), 3798–3803.
- Liemohn, M., G. Khazanov, T. Moore, and S. Guiter (1997), Self-consistent superthermal electron effects on plasmaspheric refilling, *Journal of Geophysical Research: Space Physics* (1978–2012), 102(A4), 7523–7536.
- Liemohn, M., G. Khazanov, P. Craven, and J. Kozyra (1999), Nonlinear kinetic modeling of early stage plasmaspheric refilling, *Journal of Geophysical Research: Space Physics* (1978–2012), 104(A5), 10,295–10,306.
- Mauk, B., N. J. Fox, S. Kanekal, R. Kessel, D. Sibeck, and A. Ukhorskiy (2014), Science objectives and rationale for the Radiation Belt Storm Probes mission, in *The Van Allen Probes Mission*, pp. 3–27, Springer.
- Mayaud, P.-N. (1980), *Derivation, meaning, and use of geomagnetic indices*, vol. 22, American Geophysical Union.
- Mizera, P., and G. Boyd (1982), A summary of spacecraft charging results. *Journal of Spacecraft and Rockets*, vol. 20.5, pp.438–443.
- Moldwin, M. B., L. Downward, H. Rassoul, R. Amin, and R. Anderson (2002), A new model of the location of the plasmopause: CRRES results, *Journal of Geophysical Research: Space Physics* (1978–2012), 107(A11), SMP–2.

Newell, P. T., W. J. Burke, C.-I. Meng, E. R. Sanchez, and M. E. Greenspan (1991), Identification and observations of the plasma mantle at low altitude, *Journal of Geophysical Research: Space Physics* (1978–2012), 96(A1), 35–45.

Olson, W. P. and Pfitzer, K. A. (1977), Magnetospheric magnetic field modeling, *Annual Scientific Report AFOSR Contract No F44620-75-c-0033*.

Ozhogin, P., J. Tu, P. Song, and B. Reinisch (2012), Field-aligned distribution of the plasmaspheric electron density: An empirical model derived from the IMAGE RPI measurements, *Journal of Geophysical Research: Space Physics* (1978–2012), 117(A6).

Pierrard, V., J. Goldstein, N. André, V. Jordanova, G. Kotova, J. Lemaire, M. Liemohn, and H. Matsui. (2009). Recent progress in physics-based models of the plasmasphere, *Space Science Reviews*, 145(1-2), 193–229.

Park, C. (1970), Whistler observations of the interchange of ionization between the ionosphere and the protonosphere, *Journal of Geophysical Research*, 75(22), 4249–4260.

Pavlov, A., and N. Pavlova (2005), Mechanism of the post-midnight winter night-time enhancements in NmF2 over Millstone Hill during 14–17 January 1986, *Journal of Atmospheric and Solar-Terrestrial Physics*, 67(4), 381–395.

Reeves, G., H. E. Spence, M. Henderson, S. Morley, R. Friedel, H. Funsten, D. Baker, S. Kanekal, J. Blake, J. Fennell, et al. (2013), Electron acceleration in the heart of the Van Allen radiation belts, *Science*, 341(6149), 991–994.

Reinisch, B., X. Huang, D. Haines, I. Galkin, J. Green, R. Benson, S. Fung, W. Taylor, P. Reiff, D. Gallagher, et al. (2001), First results from the Radio Plasma Imager on IMAGE, *Geophysical Research Letters*, 28(6), 1167–1170.

Reinisch, B. W., D. Haines, K. Bibl, G. Cheney, I. Galkin, X. Huang, S. Myers, G. Sales, R. Benson, S. Fung, et al. (2000), The Radio Plasma Imager investigation on the IMAGE spacecraft, in *The IMAGE Mission*, pp. 319–359, Springer.

Reme, H., C. Aoustin, J. Bosqued, I. Dandouras, B. Lavraud, J. Sauvaud, A. Barthe, J. Bouyssou, T. Camus, O. Coeur-Joly, et al. (2001), First multispacecraft ion measurements in and near the Earth's magnetosphere with the identical Cluster Ion Spectrometry (CIS) experiment, in *Annales Geophysicae*, vol. 19, pp. 1303–1354.

Richards, PG and DG Torr (1985), Seasonal, diurnal, and solar cyclical variations of the limiting H<sup>+</sup> flux in the Earth's topside ionosphere, *Journal of Geophysical Research: Space Physics (1978–2012)*, 90(A6), 5261–5268.

Roble, R. (1975), The calculated and observed diurnal variation of the ionosphere over Millstone Hill on 23–24 march 1970, *Planetary and Space Science*, 23(7), 1017–1033.

Sandel, B. R., A. L. Broadfoot, C. Curtis, R. King, T. Stone, R. Hill, J. Chen, O. Siegmund, R. Raffanti, D. D. Allred, et al. (2000), The Extreme Ultraviolet Imager investigation for the IMAGE mission, in *The Image Mission*, pp. 197–242, Springer.

Sandel, B. R., R. A. King, W. Forrester, D. L. Gallagher, A. L. Broadfoot, and C. Curtis (2001), Initial results from the IMAGE Extreme Ultraviolet Imager, *Geophysical Research Letters*, 28(8), 1439–1442.

Schunk, R., and A. F. Nagy (1978), Electron temperatures in the F region of the ionosphere: Theory and observations, *Reviews of Geophysics*, 16(3), 355–399.

Sheeley, B., M. Moldwin, H. Rassoul, and R. Anderson (2001), An empirical plasmasphere and trough density model: CRRES observations, *Journal of Geophysical Research: Space Physics (1978–2012)*, 106(A11), 25,631–25,641.

- Singh, N., and J. Horwitz (1992), Plasmasphere refilling: Recent observations and modeling, *Journal of Geophysical Research: Space Physics* (1978–2012), *97*(A2), 1049–1079.
- Singh, U., and R. Singh (1997), Study of plasmasphere-ionosphere coupling fluxes, *Journal of Atmospheric and Solar-Terrestrial Physics*, *59*(11), 1321–1327.
- Spasojević, M., H. Frey, M. Thomsen, S. Fuselier, S. Gary, B. Sandel, and U. Inan (2004), The link between a detached subauroral proton arc and a plasmaspheric plume, *Geophysical Research Letters*, *31*(4).
- Su, Y.-J., M. F. Thomsen, J. E. Borovsky, and D. J. Lawrence (2001), A comprehensive survey of plasmasphere refilling at geosynchronous orbit, *Journal of Geophysical Research: Space Physics* (1978–2012), *106*(A11), 25,615–25,629.
- Thomsen, M. (2004), Why Kp is such a good measure of magnetospheric convection, *Space Weather*, *2*(11).
- Usanova, M., A. Drozdov, K. Orlova, I. Mann, Y. Shprits, M. Robertson, D. Turner, D. Milling, A. Kale, D. Baker, et al. (2014), Effect of EMIC waves on relativistic and ultrarelativistic electron populations: Ground-based and Van Allen Probes observations, *Geophysical Research Letters*, *41*(5), 1375–1381.
- Weiss, L., R. Lambour, R. Elphic, and M. Thomsen (1997), Study of plasmaspheric evolution using geosynchronous observations and global modeling, *Geophysical Research Letters*, *24*(5), 599–602.
- Winningham, J., J. Burch, N. Eaker, V. Blevins, and R. Hoffman (1981), The Low Altitude Plasma Instrument/LAPI, *Space Science Instrumentation*, *5*, 465–475.
- Wygant, J., J. Bonnell, K. Goetz, R. Ergun, F. Mozer, S. Bale, M. Ludlam, P. Turin, P. Harvey, R. Hochmann, et al. (2014), The Electric Field and Waves instruments on the Radiation Belt Storm Probes mission, in *The Van Allen Probes Mission*, pp. 183–220, Springer.

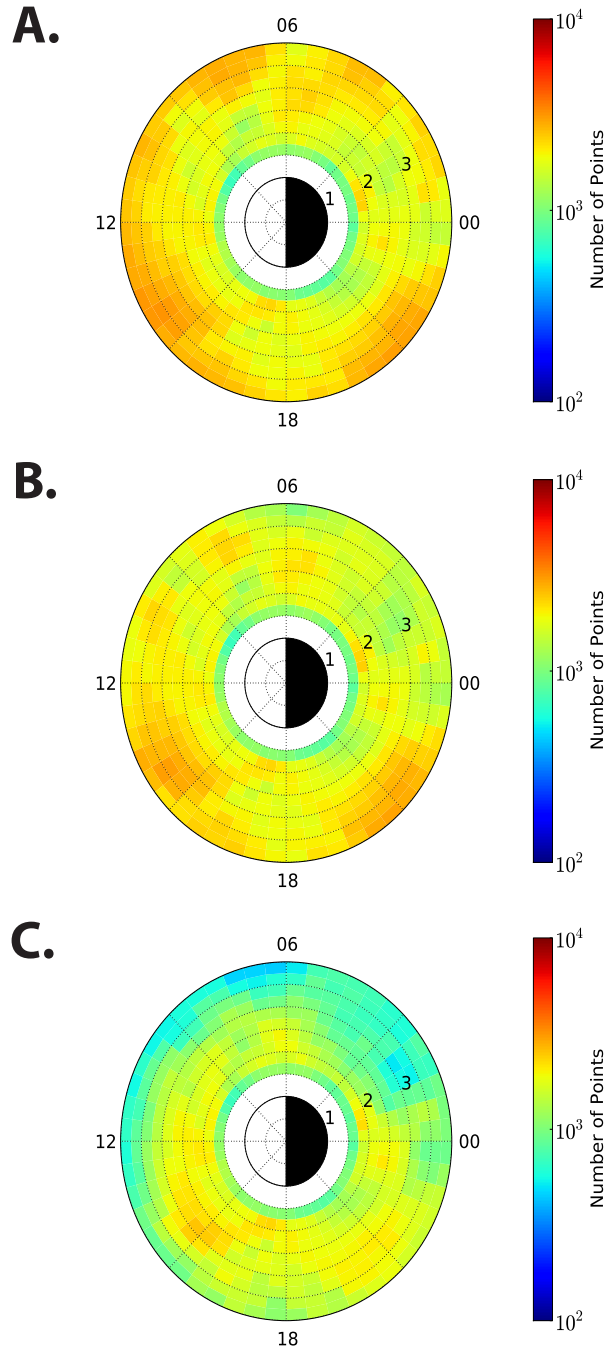


**Figure 1.** Number of measurements for the 2.2 eV energy channel on HOPE during quiet time for A)  $H^+$ , B)  $He^+$ , and C)  $O^+$  for each MLT and L-Shell bin over the 22 month period covered by our study for satellites A and B combined. The view in these equatorial plane plots is from over the North Pole with the Sun to the left and L values labeling the appropriate concentric L-Shell ring.

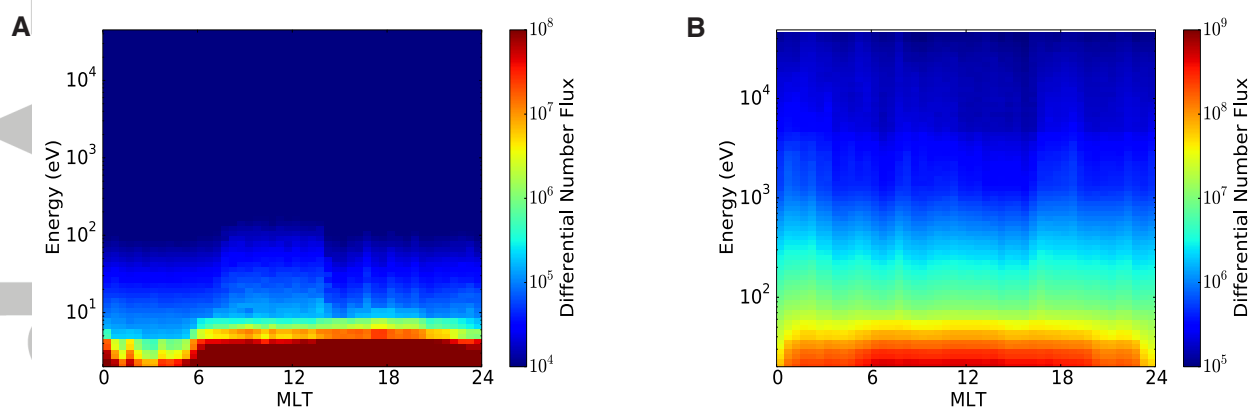


**Figure 2.** Quiet time HOPE H<sup>+</sup> (A) and electron (B) differential number flux at L=2.5 and Kp < 3 as a function of energy and MLT.

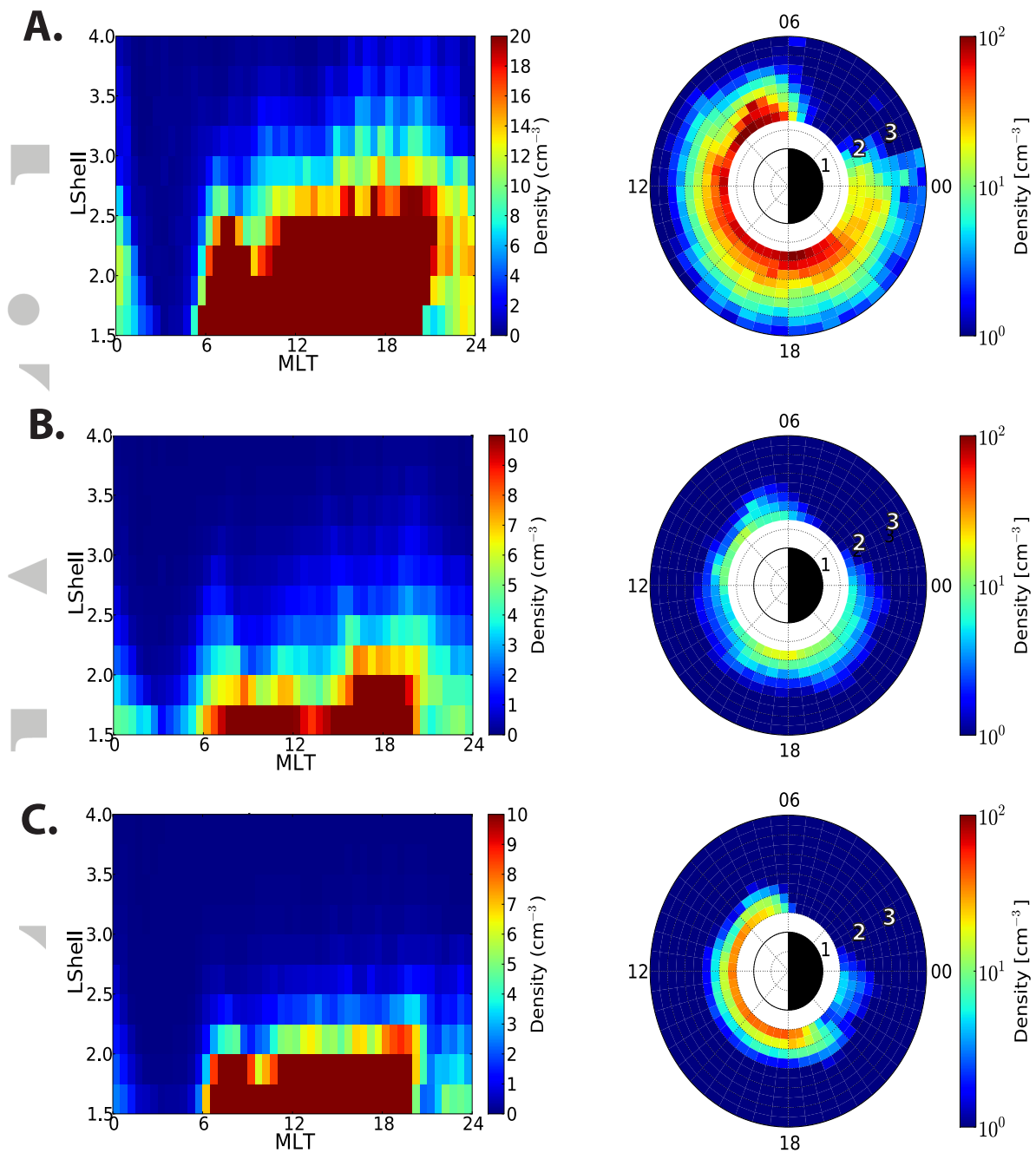


**Figure 3.** Median partial plasma density from 1-4 eV measured by HOPE during quiet times over a 22 month period for (A)  $\text{H}^+$ , (B)  $\text{He}^+$ , and (C)  $\text{O}^+$ . The density maps on the right are on a logarithmic scale, while the maps on the left are on a relative linear scale dependent on species.

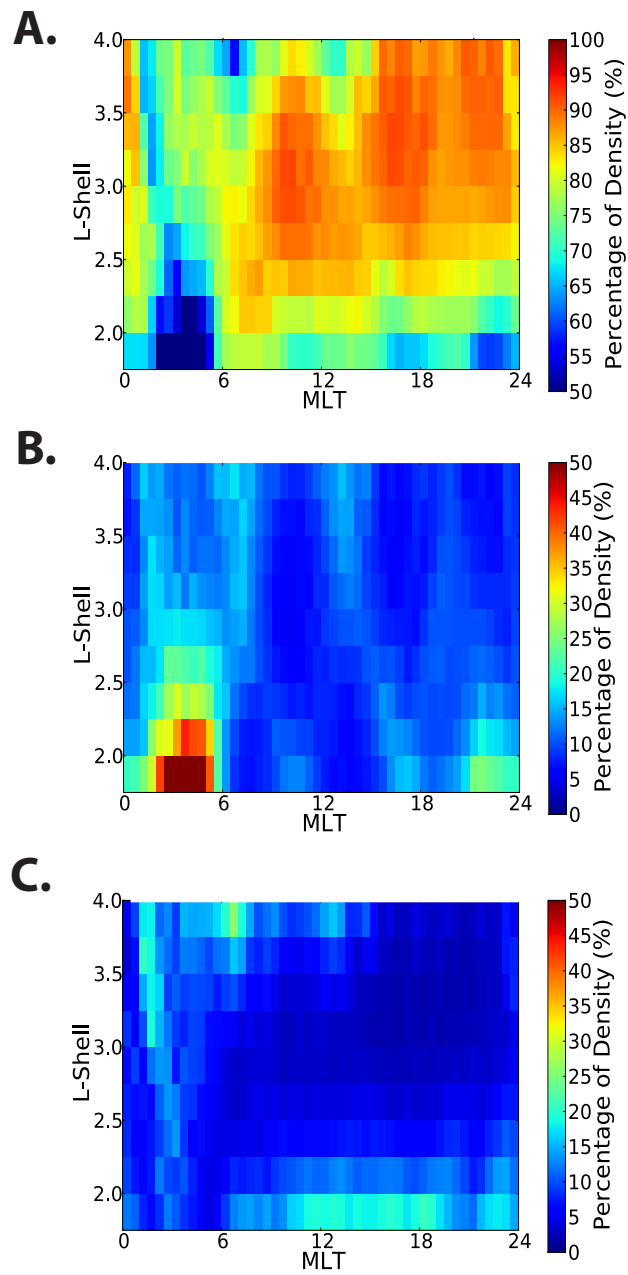


**Figure 4.** Percentage for each ion of the 1-4 eV quiet time partial plasma density at every L-Shell and MLT bin for (A) H<sup>+</sup>, (B) He<sup>+</sup>, and (C) O<sup>+</sup>

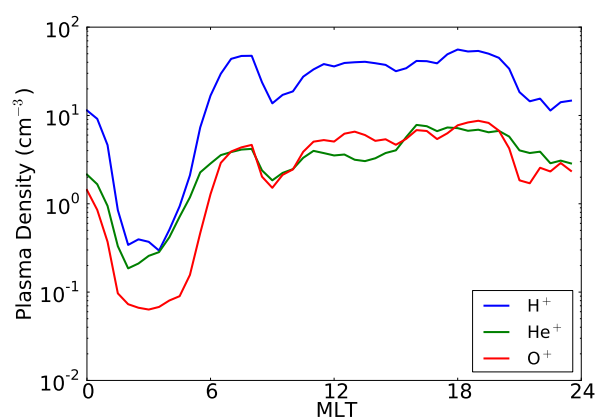


**Figure 5.** Plasma densities at L=2.0 for H<sup>+</sup> (blue), He<sup>+</sup> (green), and O<sup>+</sup> (red). H<sup>+</sup> and O<sup>+</sup> drop by 150 and 122 factors respectively, whereas He<sup>+</sup> drops by a factor of 28 across the same MLTs.

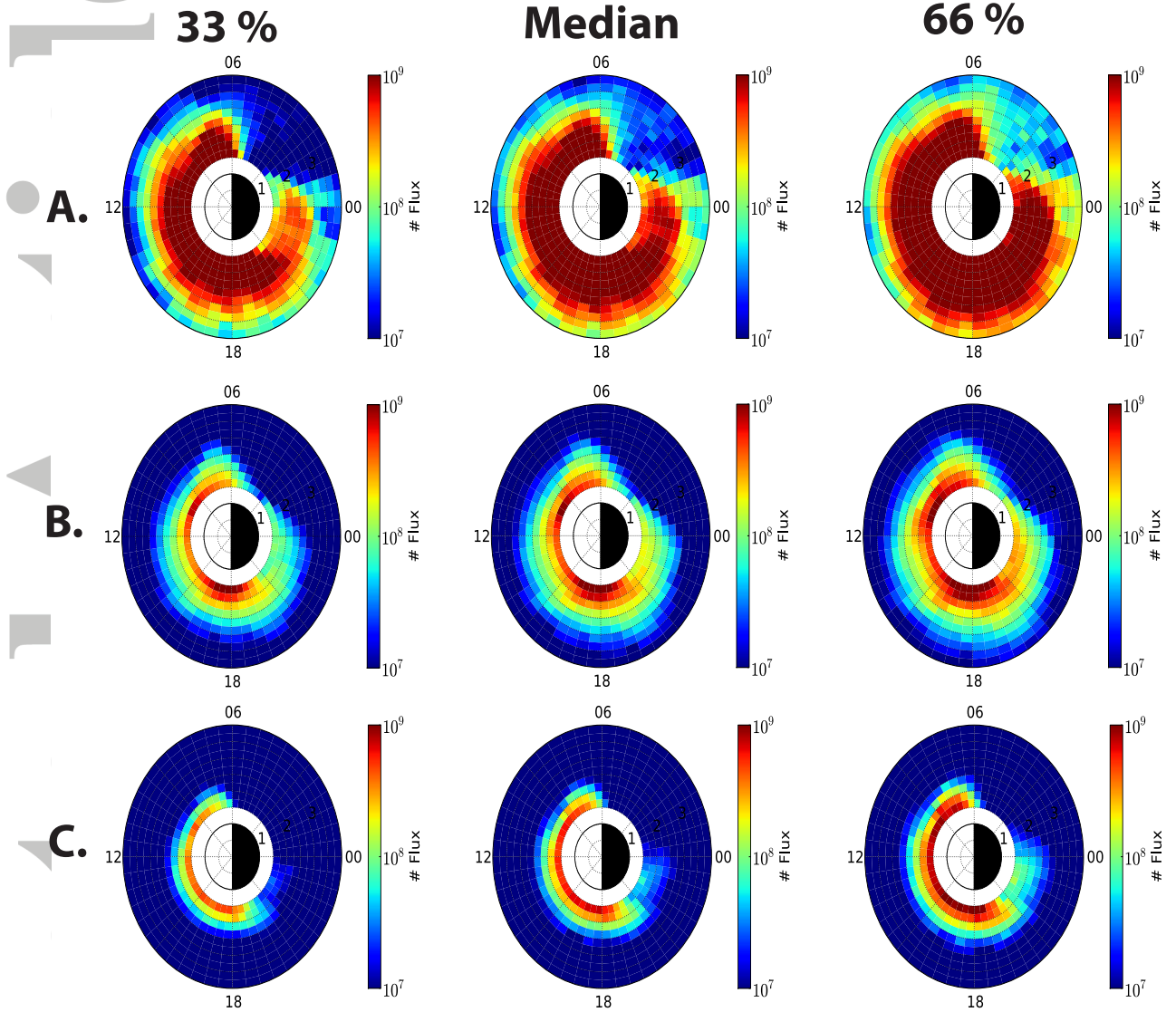


**Figure 6.** 2.2 eV flux maps for (A)  $H^+$ , (B)  $He^+$ , and (C)  $O^+$ . The 33% is the 33rd percentile of the flux measurements made in each MLT/L-Shell bin, the median column is the median flux measurement for each species, and 66% is the 66th percentile of flux measurements.

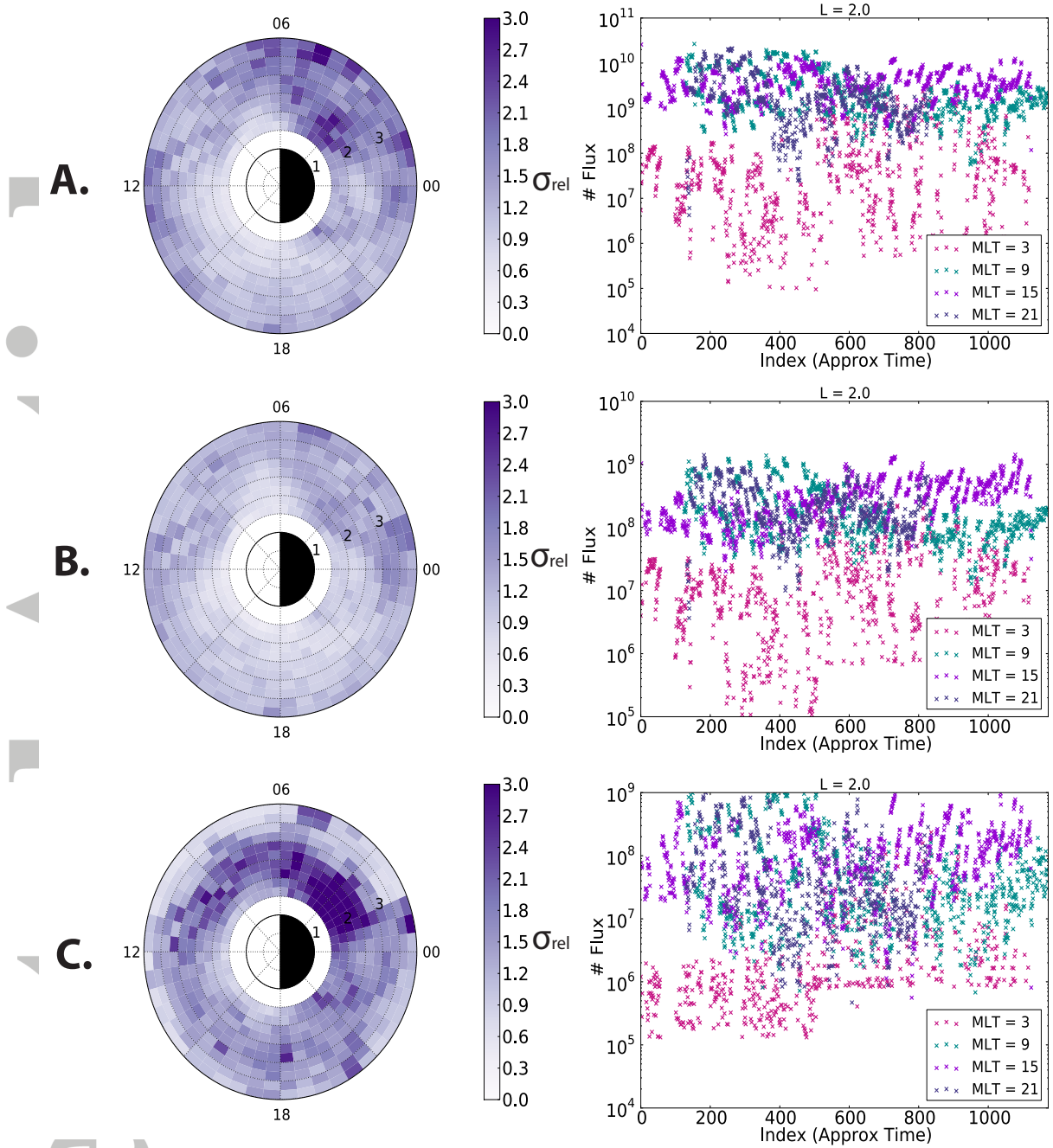


**Figure 7.** The left column gives the relative standard deviation (standard deviation / mean) in the 2.2 eV flux bins for (A)  $H^+$ , (B)  $He^+$ , and (C)  $O^+$ . The right column shows all the HOPE measurements for  $L=2.0$  of MLT=3,9,15,and 21 for each species. Both columns include both satellite A and B data. The flux measurements are ordered in time, so the label Index (Approx Time) refers the relative position of each non-zero measurement in this time ordered array.



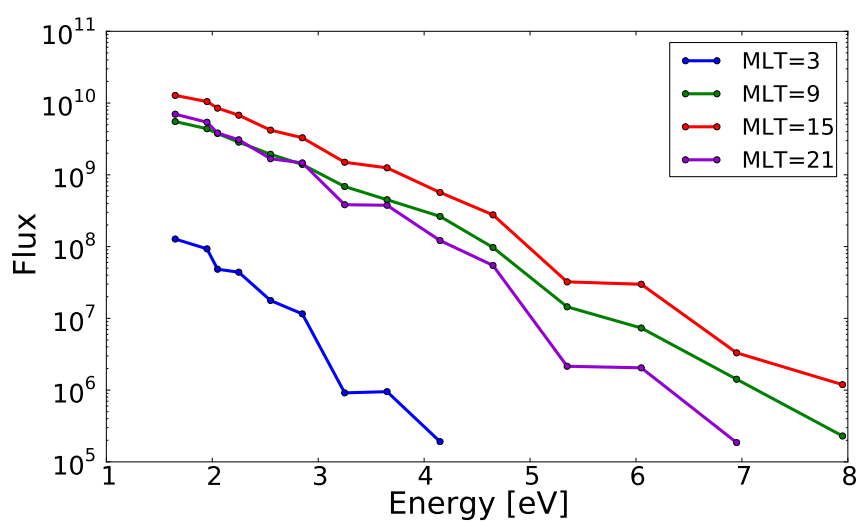


**Figure 9.** Median differential number flux measurement as a function of energy at L=2.0 for MLT=3,9,15,21.

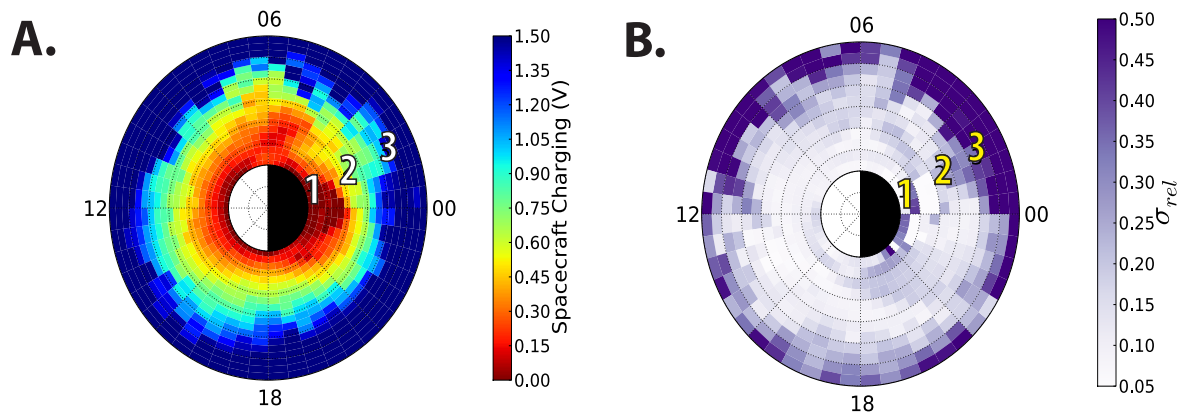


**Figure 10.** (A) is the median spacecraft potential in each 0.25 L-Shell and 0.5 MLT bin from the EFW instrument from November of 2012 to April of 2014. (B) is the relative variation (standard deviation / mean) of the spacecraft potential data shown in A.

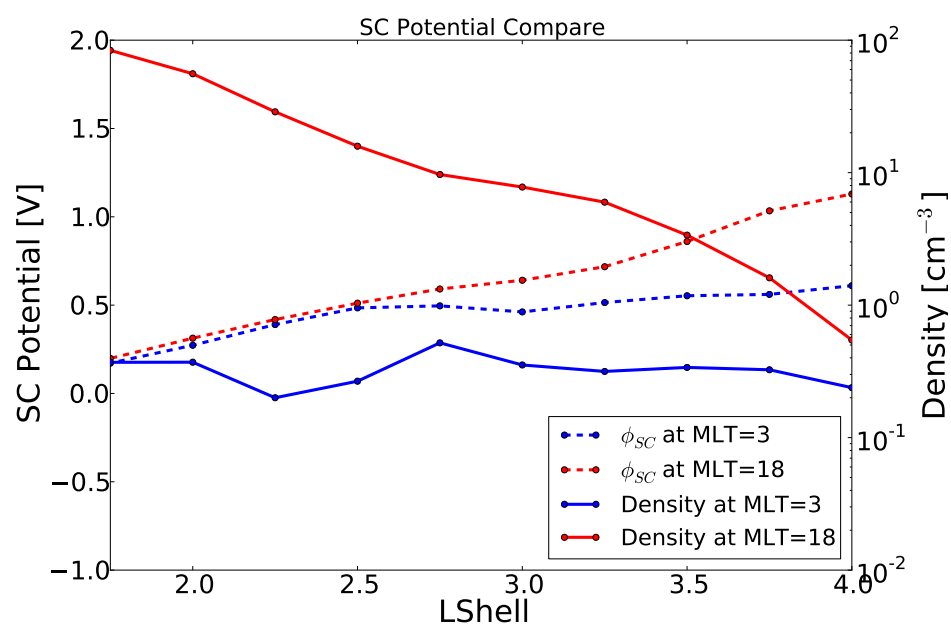


**Figure 11.** Median spacecraft potential ( $\phi_{SC}$ ) from L-Shell 1.75 to 4.0 at MLT = 3 and MLT = 18 compared with median partial plasma densities from the same bins.

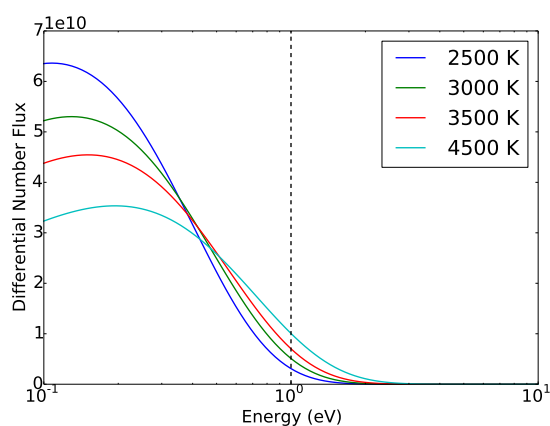


**Figure A1.** Differential number flux for a Maxwellian  $H^+$  distribution as a function of energy at different plasmaspheric temperatures. The dotted black line indicates 1 eV, the minimum HOPE measurement energy. We assume a total number density of  $1800 \text{ cm}^{-3}$  as given by *Chappell* [1972].